The effects of river run-off on water clarity across the central Great Barrier Reef

K.E. Fabricius [a,*], M. Logan [a], S. Weeks [b], J. Brodie [c]

[a] Australian Institute of Marine Science, PMB No. 3, Townsville, Queensland 4810, Australia
[b] Biophysical Oceanography Group, School of Geography, Planning and Environmental Management, University of Queensland, Brisbane 4072, Australia
[c] Centre for Tropical Water & Aquatic Ecosystem Research, James Cook University, Townsville, Queensland 4811, Australia

ARTICLE INFO

ABSTRACT

Changes in water clarity across the shallow continental shelf of the central Great Barrier Reef were investigated from ten years of daily river load, oceanographic and MODIS-Aqua data. Mean photic depth (i.e., the depth of 10% of surface irradiance) was related to river loads after statistical removal of wave and tidal effects. Across the ∼25,000 km² area, photic depth was strongly related to river freshwater and phosphorus loads (R^2 = 0.65 and 0.51, respectively). In the six wetter years, photic depth was reduced by 19.8% and below water quality guidelines for 156 days, compared to 9 days in the drier years. After onset of the seasonal river floods, photic depth was reduced for on average 6–8 months, gradually returning to clearer baseline values. Relationships were strongest inshore and midshelf (∼12–80 km from the coast), and weaker near the chronically turbid coast. The data show that reductions in river loads would measurably improve shelf water clarity, with significant ecosystem health benefits.

1. Introduction

Water clarity or transparency is a key factor for marine ecosystems, affecting the resource supply for photosynthetic organisms and filter feeders. Coral reefs and seagrass meadows are built by photosynthetic organisms, and are therefore highly sensitive to changes in water clarity. Reduced water clarity leads to reduced coral biodiversity and increased macroalgal cover (De'ath and Fabricius, 2010), shifts in communities towards heterotrophic filter feeders (Birkeland, 1988), and a proliferation of filter-feeding macro-bioreordering organisms that weaken the structural integrity of coral reefs (LeGrand and Fabricius, 2011). Prolonged shading from reduced water clarity also limits the depth distribution of coral reefs, with an apparent threshold at ∼6–8% of surface irradiance as absolute minimum for reef development (Cooper et al., 2007), and the lower depth limit of seagrasses (Duarte, 1991; Collier et al., 2012).

It is clearly established that the water clarity in shallow shelf seas is adversely affected by sediment resuspension from waves and currents (Larcombe et al., 1995; Wolanski et al., 2005; Piniak and Storlazzi, 2008; Storlazzi and Jaffe, 2008; Storlazzi et al., 2009; Fabricius et al., 2013). However it remains poorly understood for how long and by how much river runoff of sediments and nutrients will affect water clarity in shelf seas. For the Australian Great Barrier Reef (GBR), terrestrial runoff is of great concern (Brodie et al., 2011; Brodie and Waterhouse, 2012). Over 30 major rivers discharge sediments and nutrients from increasingly developed catchments into the shallow and wide continental shelf sea, which contains the >3000 coral reefs, ∼40,000 km² of subtidal inter-reefal seagrass meadows and many other interreefal marine habitats that constitute this large World Heritage area. Rivers now discharge 17 million tonnes of suspended sediments, 80,000 tonnes of nitrogen, and 16,000 tonnes of phosphorus annually into the GBR, an 3–8-fold increase compared to pre-European times (Kroon et al., 2012). Satellite images derived from the Moderate Imaging Spectroradiometer (MODIS) document reduced water clarity within the river plumes, and show that long-shore currents transport their particulate loads (silt, clay, plankton and organic rich sediment flocs) for tens to hundreds of kilometers northwards away from the river mouths, and typically remain initially within ∼5 km of the coast (Brodie et al., 2010; Bainbridge et al., 2012). After the plume has dissipated, these newly imported sediments continue to undergo repeated cycles of resuspension and deposition, until they eventually settle in wave-sheltered embayments or offshore beyond the depth of wave resuspension (Orpin et al., 2004; Wolanski et al., 2008; Bainbridge et al., 2012). Nepheloid flows and tropical cyclones can shift significant amounts of coastal sediments into deeper offshore waters (Gagan

* Corresponding author.
E-mail address: k.fabricius@aims.gov.au (K.E. Fabricius).

et al., 1990; Wolanski et al., 2003). Seafloor sediments are dominated by terrigenous materials from the shore to about 20 m depth, but consist mostly of biogenic carbonates further offshore (Belperio and Searle, 1988).

Substantial recent management efforts to reduce the terrestrial runoff of nutrients and sediments into the GBR have led to small but significant reductions in end-of-river sediment and nutrient loads (State of Queensland, 2013). However, both the intra- and inter-annual time-scale of burial or export of such newly imported fine sediments (with residency times beyond that of acute floods) remain poorly understood. Water clarity is typically low in the shallow coastal and inshore zone (De'ath and Fabricius, 2010; Weeks et al., 2012), but within that zone, it is up to 10-fold lower near, compared to away from river mouths, suggesting a long-term accumulation of river derived resuspendible sediments on the seafloor (Fabricius et al., 2013).

Newly imported materials are assumed to be retained on the shelf for decades to centuries, suggesting that the effects of water quality improvements may become measurable within the marine environment only at a time scale of decades (Brodie et al., 2012; The State of Queensland and Commonwealth of Australia, 2009). Fabricius et al. (2013) documented that water clarity in the GBR after floods returned to clear values within weeks to years, rather than years to decades. However, that study was limited to coastal and inshore waters and the three year-long instrumental record was too short to assess inter-annual variation in water clarity. The present study significantly expands this work, and used a novel approach (outlined below) to assesses the relationship between terrestrial runoff and daily changes in water clarity across the ~120 km wide continental shelf of the GBR over a period of 10 years.

'Photic depth' ($Z_{\%}$; unit: m) is a measure to quantify light availability (as photosynthetically active radiation, PAR) relative to the light at the water surface. For example, the water depth of the euphotic zone, $Z_{1\%}$, reflects the depth where PAR is 1% of its surface value, and $Z_{10\%}$ is the photic depth for 10% of surface PAR (Lee et al., 2007; Weeks et al., 2012). Photic depth depends on the light attenuation in the water column, which is traditionally quantified from remote sensing data as the diffuse attenuation coefficient of the downwelling spectral irradiance at 490 nm wavelength, K_{d490}, or the photosynthetically available radiation, K_{dPAR} (Saulquin et al., 2013). Light attenuation is diminished by suspended abiotic and biotic particulate matter (esp. clay- and fine silt sized particles) and some dissolved substances. Photic depth can therefore be used as a measure of water clarity (Lee et al., 2007).

In optically complex waters, semi-analytical algorithms typically provide better results than traditional empirical algorithms to convert the ocean color signal into biogeochemical quantities (IOCCG, 2006). Lee et al. (2002, 2007) derived photic zone depths ($Z_{1\%}$, $Z_{10\%}$ and $Z_{50\%}$) semi-analytically from spectral remote-sensing reflectance using a model based on the inherent optical properties of water and a suite of in situ measurements. $Z_{1\%}$ and $Z_{10\%}$ values were found to be, on average, within 14% of the in situ values, both within complex coastal and shelf waters as well as oceanic waters, and across different seasons. Historically, ocean transparency has been most often measured using Secchi disk as a useful index of water quality. Doron et al. (2011) adapted Lee's algorithm to estimate Secchi depth from satellite ocean color data using an extensive set of coincident satellite and in situ measurements (>400 matchups) from both coastal and oceanic waters. A recent study evaluated K_{dPAR}, $Z_{1\%}$ and K_{d490}, derived with three bio-optical algorithms applied to Moderate Imaging Spectroradiometer (MODIS) and Sea-viewing Wide Field-of-view Sensor (SeaWiFS) observations, using optical data from the coastal waters off South Florida and the Caribbean Sea (Zhao et al., 2013). The algorithm by Lee et al. (2007) showed the overall best performance, while empirical

algorithms performed well for clear offshore waters but underestimated K_{dPAR} and K_{d490} in coastal waters. Zhao et al. (2013) suggested their findings lay the basis for synoptic time-series studies of water quality in coastal ecosystems, although more work is required to minimize bottom interference in optically shallow waters.

This study uses a new approach to assess the relationships between the terrestrial runoff of freshwater and its associated fine sediments and nutrients to the daily to inter-annual variation in water clarity, using the central section of the shallow GBR continental shelf as a model system. The study was based on 10 years of remote sensing and environmental data (2002–2012), a new GBR-validated photic depth algorithm for MODIS-Aqua data (Weeks et al., 2012) and statistical models. The study shows that annual mean water clarity in the central GBR is strongly related to discharges by the large Burdekin River. The study then assessed the spatial extent (inshore to ~120 km offshore) and the duration of reduction in water clarity beyond the duration of the flood plumes. The results suggest that reductions in the sediment and nutrient loads of the Burdekin River will likely result in significantly improved water clarity downstream of the river mouth and across much of the central GBR, both during the wet season and throughout the following dry season.

2. Methods

2.1. MODIS data: photic depth

Water clarity was calculated by applying a GBR-validated 'photic depth' algorithm to MODIS-Aqua, i.e., determining the depth where 10% of the surface light level is still available (GBR $Z_{10\%}$). The method is fully described in Weeks et al. (2012). In brief: GBR $Z_{10\%}$ was calculated with the algorithm of Lee et al. (2002, 2007) based on the regression coefficients of satellite data against GBR Secchi depth data. Many of the >5000 records of Secchi depth (collected by the Australian Institute of Marine Science and the Queensland Department of Primary Industries and Fisheries between 1994–1999 and 1992–2012) pre-dated the MODIS-Aqua satellite data (2002–2012), hence both MODIS-Aqua and SeaWiFS data (1997–2010) were used. Satellite to in situ "matchups" ($Z_{10\%}$) for the Secchi data were acquired from the NASA Ocean Biology Processing Group. Stations in optically shallow water, where the signal is affected by light reflection from the sea floor, were excluded. A Type II linear regression of log-transformed satellite and Secchi values was applied, to then estimate GBR $Z_{10\%}$ as:

$$\text{GBR } Z_{10\%} = 10 \wedge [(\log_{10}(Z_{10\%}) - a_0)/a_1] \tag{1}$$

where a_0 and a_1 are slope and intercepts of satellite data against Secchi (values: 0.518 and 0.811 for SeaWiFS, and 0.529 and 0.816 for MODIS-Aqua). GBR $Z_{10\%}$ was implemented into the NASA satellite processing software (SeaDAS) and applied to the full time series of MODIS-Aqua data (01 July 2002 to 21 November 2012).

The large Burdekin River with its 133,400 km^2 catchment area is the single greatest source of suspended sediments into the GBR lagoon (mean: 4 million tonnes yr^{-1}, representing ~25% of total loads entering into GBR; Kroon et al., 2012). A mask was generated for the continental shelf off the Burdekin Natural Resource Management region (~17.9–20.1°S and 146.3–149.3°E), extending from the shore to the 200 m depth contour, and excluding coral reefs (Fig. 1). To the best of our knowledge, grid points in optically shallow water were also excluded. The final data contained 25,621 grid points each covering a 1-km^2 area. Data availability varied greatly between days and months due to cloud cover.
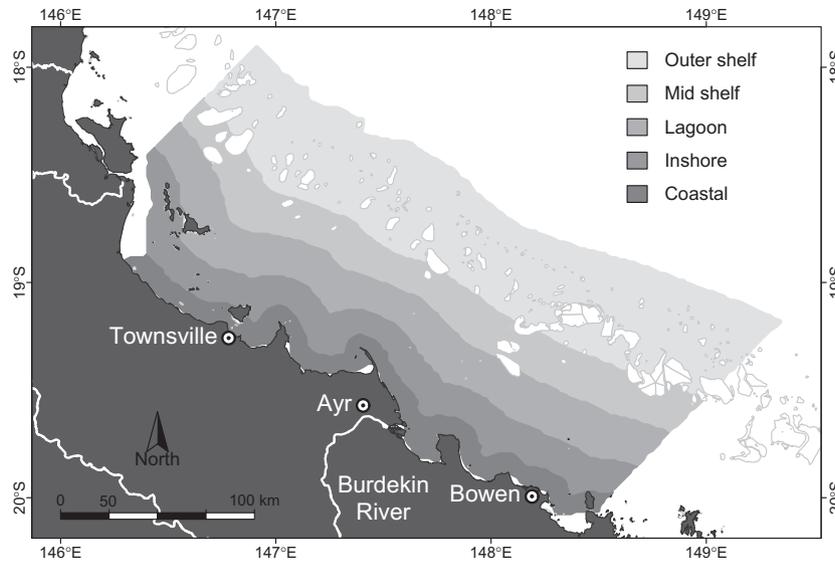
Fig. 1. Study region, and the five bands across the continental shelf, defined by their distance proportional to the width of the shelf: coastal (0–0.1 across), inshore (0.1–0.25 across), lagoon (0.25–0.45 across), midshelf (0.45–0.65 across), and outer shelf (>0.65 across).

2.2. Environmental data

Environmental data were obtained as follows: bathymetry data (meters below mean sea level) for each grid point were obtained from a high-resolution digital elevation model for the GBR at a resolution of 0.001-arc degrees (about 100 m) (Beaman, 2012). Daily data of freshwater discharge volumes of the Burdekin, Houghton, Ross and Black Rivers were provided by the State of Queensland, Department of Environment and Heritage Protection (DEHP). Annual loads of suspended solids, total nitrogen and total phosphorus of the Burdekin River were obtained for 2003–2009 from Kuhnert et al. (2012) and for 2010–2011 from DEHP at the Clare/Home Hill gauge and monitoring station (Table 1). Hourly data on wave heights and wave frequencies were obtained from the DEHP from a wave rider buoy in the center of the study region (8 km off the coast, at 19.1487° latitude South, 147.0576° longitude East). Daily rainfall data from Townsville Airport station and hourly wind speed data from Cape Ferguson were obtained from the Australian Bureau of Meterology (http://www.bom.gov.au/oceanography/projects/abslmp/data/index.shtml). Daily tidal amplitudes as a proxy for tidal currents (one daily value for the whole region) were calculated from hourly predicted sea level data derived from a DEHP-operated storm tide gauge site in Townsville Harbour (19.2538°S, 146.8295°E). Gaps in the tidal range data were input

from estimates generated from a harmonic tide clock and tide predictor (Flater, 2007) after correcting for an offset calculated over all available tide measurements.

2.3. Statistical analyses

Relative distance across (proportional to the width of the continental shelf) and along the shelf was calculated for each grid point. Daily and annual estimates of photic depth were calculated as means of all grid points, and separately within each of five cross-shelf transects (coastal: 0–0.1 across the shelf, inner: 0.1–0.25, lagoon: 0.25–0.45, midshelf: 0.45–0.65, outer shelf: >0.65 across; Fig. 1). The distance of the boundaries between these arbitrary bands varied with latitude, approximating ~8–13 km from the shore to the inshore, ~27–43 km from the inshore to the lagoon, ~55–60 km from the lagoon to the midshelf, and ~67–85 km from the midshelf to the outer shelf band. Annual means were calculated based on 'water years' (01 October to 30 September), accounting for the wet season in the GBR that extends from November to about April the following calendar year.

The first set of analyses (Fig. 2) focused on annual values (with annual values based on water years 2). Annual mean photic depth (calculated across the entire region) was correlated against the annual total Burdekin River freshwater discharge volume, total

Table 1

Annual mean values of discharges of the Burdekin River by freshwater volume, total suspended solids (TSS: data sources: 2003–2009: Kuhnert et al. (2012), 2010–2011: Department of Environment and Heritage Protection (DEHP)), total nitrogen (TN), and total phosphorus (TP). Within the Great Barrier Reef: annual mean values of photic depth and the environmental drivers, wave height, wave frequency, and tidal range. Data are based on 'water years' (i.e., the water year 2003 represents the period 1st October 2002 – 30th September 2003).

| Water year | Burdekin River loads | | | | GBR | | | |
	Freshwater volume (10^3 ML)	TSS (1000 t)	TN (t)	TP (t)	Photic depth (m)	Wave height (m)	Wave frequency (s)	Tidal range (m)
2003	514	755	NA	NA	10.8	0.60	3.57	2.09
2004	513	384	NA	NA	11.3	0.65	3.60	2.10
2005	548	4338	4500	1100	10.6	0.68	3.44	2.12
2006	541	884	1600	185	11.6	0.63	3.50	2.07
2007	711	7195	7826	2685	11.3	0.62	3.54	2.08
2008	935	14,806	26,528	7523	10.4	0.65	3.53	2.12
2009	939	10,855	18,504	5375	10.4	0.58	3.55	2.14
2010	717	2485	6411	2213	9.93	0.64	3.70	2.08
2011	1258	6167	21,450	8410	8.94	0.59	3.53	2.14
2012	881	NA	NA	NA	10.4	0.61	3.61	2.11
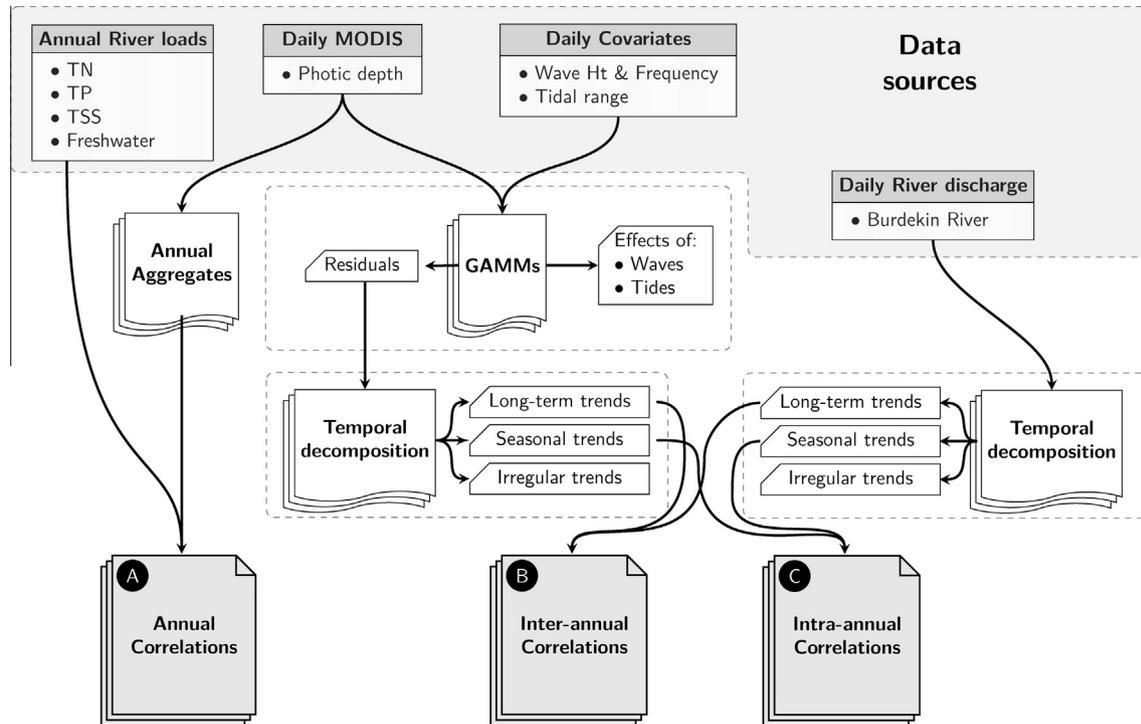
Fig. 2. Diagram representing a flow chart of the individual steps taken in the statistical analyses.

river loads of suspended solids (TSS), total nitrogen (TN) and total phosphorus (TP).

The second set of analyses was based on daily values. Time series traces of photic depth and the environmental data were produced for initial exploration and to confirm the existence of cyclical (seasonal) patterns (Electronic Supplement, Fig. S1). Wind speed was highly correlated with wave height and wave frequency. Daily rainfall was highly correlated with the Burdekin River discharges, and so were the discharges of the much smaller Houghton, Ross and Black Rivers. Only wave height, wave frequency and Burdekin River flow, which are the most direct predictors for water clarity, were therefore retained in the final model.

Cross-correlation lags between daily photic depth and the main environmental drivers were calculated to determine the potential scale and pattern of temporal offsets. These cross-correlations revealed that there was a substantial and blunt (prolonged) lag associated with Burdekin River discharge (Fig. 3), suggesting that any potential causal links between photic depth and river discharge were delayed and accumulative over prolonged periods rather than instantaneous pulses. Lags of the response in photic depth to the other environmental drivers were negligible.

Next, to remove the effects of bathymetry, wave height, wave frequency and tidal range on photic depth, we fitted generalized additive mixed effects models (GAMMs; Wood, 2006), using the mgcv (Wood, 2006, 2011) package in R 2.15.1 (R Development Core Team, 2013). GAMMs allow flexible modeling of non-linear relationships by incorporating penalized regression spline types of smoothing functions into the estimation process. The degree of smoothing of each term (and by extension, the estimated degree of freedom of each smoother) is treated as a random effect, and thus estimable via its variance as with other effects in a mixed modeling structure (Wood, 2006). Smoothing functions were represented by penalized β-splines (Eilers et al., 1996). Spatial and temporal autocorrelation was explicitly modeled by including the cross-shelf bands as random effects and incorporating a first-order autoregressive correlation structure (Pinheiro and Bates, 2000).

Normality was checked and ln-transformations were used to normalize photic depth, wave height and wave frequency. The data from July to September 2002 were excluded from the correlation analysis as the MODIS-Aqua data series started 01 July 2002 and hence represented an incomplete water year (starting 01 October). Modeling against a Gaussian distribution greatly reduced the computational effort and convergence issues compared to a Gamma distribution.

The residuals from these GAMM (which thus reflect the photic depth signal after the extraction of wave, tidal and bathymetry signals) were then decomposed to derive both the inter-annual (2003–2012) and intra-annual trends (i.e., seasonal based on 365.25 day cyclicity) in photic depth (Fig. 2). Seasonal decomposition applies a smoother (typically either a moving average or locally weighted regression smoother) through a time series to separate periodic fluctuations due to cyclical reoccurring influences and long-term trends (Kendall and Stuart, 1983). Such decomposition is represented mathematically as:

$$Y_t = f(S_t, \ T_t, \ E_t) \tag{2}$$

where Y_t, S_t, T_t and E_t are the observed value, seasonal trend, long-term trend and irregular (residual) components, respectively, at time t. Additive decomposition was considered appropriate here since the amplitude of seasonal fluctuation remained relatively constant over time. As the residuals from a Gaussian model are zero-centered and since the response variable was log-transformed, the residuals are on a log scale. Thus following temporal decomposition, seasonal cycles and long-term trends were re-centered around mean GAMM fitted values, and transformed back into the original photic depth scale via exponentiation. Patterns in daily Burdekin River discharge values were also decomposed both for seasonal and long-term trends (Fig. 2). Long-term water clarity trends were hence cross-correlated against long-term river discharge trends. Effect sizes (rate of change in long-term water clarity per unit change in long-term discharge) were expressed as a percentage of initial water clarity, and R^2 values were calculated.
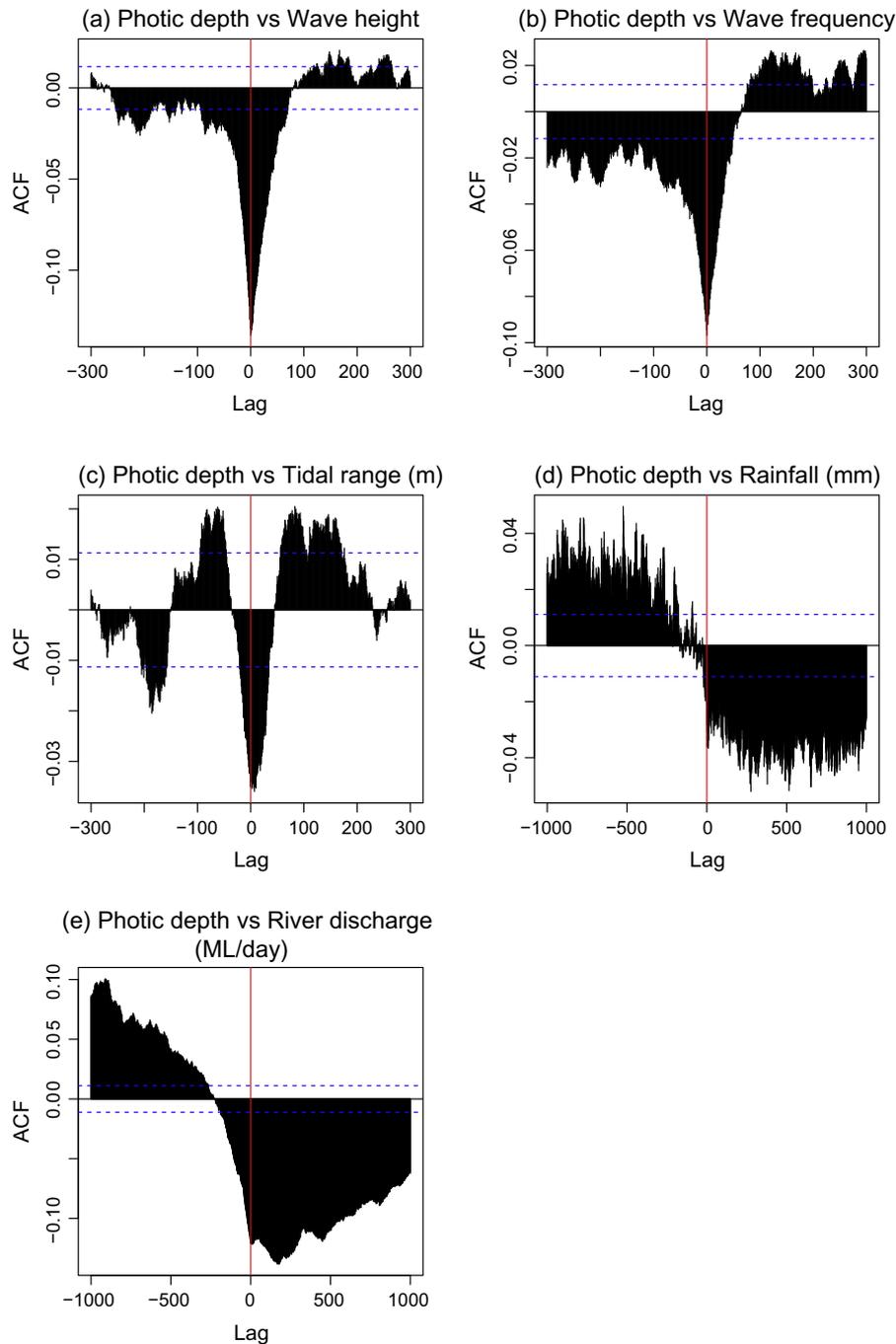
Fig. 3. Cross-correlation lags for daily photic depth values against the environmental drivers, wave height, wave frequency, tidal range, rainfall and Burdekin River discharge.

To explore spatial differences in the associations of photic depth and Burdekin River discharge, GAMMs and seasonal decompositions were also performed separately for each cross-shelf band (coastal, inner, lagoon, midshelf and outer shelf). In each case, photic depth data comprised daily measurements averaged across all points within that band. To explore temporal differences in photic depth between wet and dry years, the analyses were also performed separately for dry (2003–2006) and wet (2007–2012) years.

3. Results

Spatial and seasonal differences in photic depth were pronounced (Table 2). Annual mean photic depth was almost four times greater in the offshore compared with the coastal transect (15.4 m vs. 3.9 m). Across the whole shelf, monthly mean photic depth was 32% greater in the period August to December than in March to June. Seasonal differences were greatest in the lagoon (40% reduction), intermediate in the inshore and midshelf bands (35% and 34.3%, respectively), and weakest in the coastal and outer shelf bands (23% and 22%). The seasonal reductions were 80% and 55% greater in the lagoon and in inshore and midshelf waters than in the outer shelf waters.

Annual mean photic depth, unadjusted for any of the environmental drivers, was strongly related to annual Burdekin discharges of freshwater (R^2 = 0.65; Fig. 4). The relationship was only slightly weaker to the river loads of total phosphorus (R^2 = 0.51), but much weaker to total nitrogen (R^2 = 0.33) and total suspended solids (R^2 = 0.14). TSS, TN and TP were all highly correlated to each other

Table 2
Monthly and annual median photic depth (in meters) as a measure of water clarity for each cross-shelf band and the whole central Great Barrier Reef region. Also shown is the percent reduction in photic depth during flood times in the wet season (average March–June) compared with the dry season (August–December), and this reduction as a proportion of the reduction observed in the outer shelf band.

Shelf	January	February	March	April	May	June	July	August	September	October	November	December	Annual mean	Reduction wet vs. dry (%)	Perc. of outer shelf
Coastal	4.4	3.6	3.3	3.1	3.4	3.7	3.9	4.3	4.11	4.0	4.6	4.9	3.9	23.0	104
Inshore	9.0	7.7	6.3	6.3	6.7	7.3	8.7	10.5	10.9	9.5	9.7	10.4	8.6	34.8	157
Lagoon	13.4	12.2	9.7	9.6	9.9	10.8	13.0	16.1	17.9	16.5	15.7	17.1	13.5	40.0	180
Midshelf	13.9	12.3	10.7	10.5	10.9	11.8	13.3	16.1	18.3	16.7	16.0	16.4	13.9	34.3	155
Outer shelf	15.4	14.2	13.5	13.6	13.4	13.6	14.0	16.2	18.5	17.5	17.6	17.1	15.4	22.2	100
Regional mean	11.2	10.0	8.7	8.6	8.9	9.4	10.6	12.6	13.9	12.9	12.7	13.2	11.1	31.9	144

and to the total freshwater volume, compromising the ability to further investigate the relative contribution of each of these factors to the observed reduction in water clarity.

Cross-correlation lags for daily photic depth in relation to the wave height, wave frequency and tidal range all suggested a lag of 0 days (Fig. 3). This indicated that waves and tides affect water clarity more or less instantaneously, and that the effects were maintained for only a few days. In contrast, cross-correlation lags between photic depth and Burdekin River discharge had more complex patterns, suggestive of a lag of up to ~100 days. This suggested that river discharges appeared to affect water clarity with a delayed onset, and were maintained over several months.

A GAMM fitted to the daily data (mean photic depth across the whole 25,000 km^2 study region) also showed strong instantaneous effects of wave height, wave frequency and tidal range and bathymetry on photic depth. Burdekin discharge was not included in this analysis of instantaneous effects, accounting for the observed longer lag phase between discharge and photic depth. As expected, mean daily wave height and bathymetry were very strong predictors of daily photic depth (Table 3). Daily tidal range contributed in a minor way, and daily wave frequency (which is strongly related to wave height) was the weakest predictor. The model explained 74% of the variation in the data. The following analyses were therefore conducted on the residual daily photic depth values (for the whole region, and for each cross-shelf band), after having removed the effects of wave height, wave frequency and tidal range.

To further investigate inter-annual trends, region-wide seasonal decomposition was used to remove the seasonal components of the time series. Once seasonal cycles were removed, the analysis showed pronounced discrete minima in standardized photic depth,
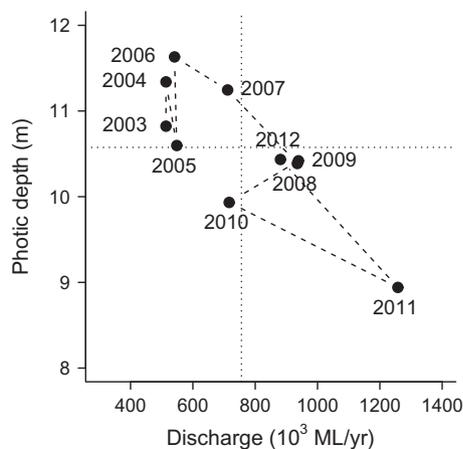
Table 3
Relationship of photic depth (daily means of all grid points) to wave height, wave frequency, tidal range and bathymetry. Output from a generalized additive mixed effects model.

	Ref.df	F	P
Wave height	4.24	51.62	<0.0001
Wave frequency	1.51	7.23	0.0022
Tidal range	1.00	40.98	<0.0001
Bathymetry	3.90	2231.47	<0.0001

many of which seemed to be aligned with the spikes in the raw and unadjusted maxima of the Burdekin freshwater discharge volumes (Electronic Supplement, Fig. S2). Across years, mean photic depth was strongly related to Burdekin discharges (Fig. 5, $R^2 = 0.65$). Burdekin discharges increased from low to higher values, with some periods of minor declines in between and a maximum in the year 2011. At the same time, there was a distinct gradual decline in mean photic depth (from 8.5 m to 6.5 m), with some periods of minor recovery in between, and a minimum in the year 2011.

To determine how the suggested river influence extended across the shelf, the above analyses were repeated for the five cross-shelf transects separately (Fig. 6). The relationship of photic depth to Burdekin discharge values was strong for inshore, lagoon and midshelf bands (correlation coefficients: inshore: $R^2 = 0.61$, lagoon: $R^2 = 0.64$, midshelf: $R^2 = 0.56$), weaker within the coastal strip that is chronically turbid ($R^2 = 0.45$), and very weak for outer shelf waters ($R^2 = 0.24$).

The intra-annual relationship between river discharge and the residuals of photic depth was also strong. Averaged across the ten years, the seasonal Burdekin River started discharging in January, peaked in March, declined to low levels in April, and remained dry for the rest of the year (Electronic Supplement, Figs. S1 and S2). There were strong differences in the freshwater discharge volumes of the Burdekin River between water years, with four dry water years (2003–2006) being followed by six wet years with on average 64.4% greater discharge volumes (2007–2012; Table 1). Data were therefore separated into the four dry and six wet water years. Averaged across the whole continental shelf, mean daily photic depth was 19.8% lower in the wet compared to the dry water years. The timing of the individual peaks and troughs, and the number of days of decline and recovery were relatively similar between these two sets of years, however the decline was more pronounced in the wet compared to the dry years (Fig. 7). In the wet years, regional mean photic depth dropped below 10 m photic depth (a regional water quality guideline threshold; Great Barrier Reef Marine Park Authority, 2009) for 156 days, whereas in the dry years it was below 10 m for an average of 9 days per year. Standardized photic depth (i.e., the residuals from the GAMMs after removal of the environmental drivers) was highest in September to December, and steeply declined from December/January to April/May. From

Fig. 4. Plot of annual mean photic depth in the central GBR against total annual freshwater discharge by the Burdekin River (in 10^3 ML) from 2003 to 2012. Annual values calculated based on water years (1st October – 30th September).
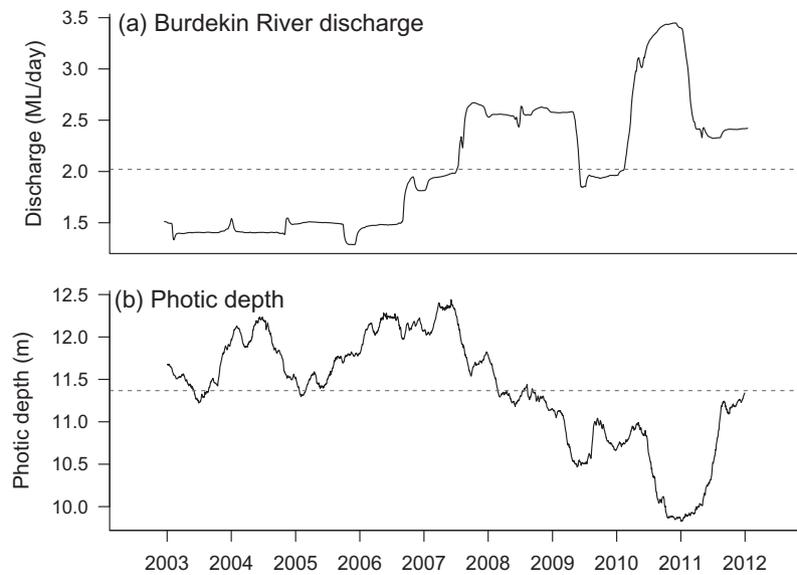
Fig. 5. Detrended values for average daily Burdekin River discharges (a) and daily mean photic depth across the central GBR (b), between the years 2002 and 2012. Horizontal dashed lines indicate long-term mean values.
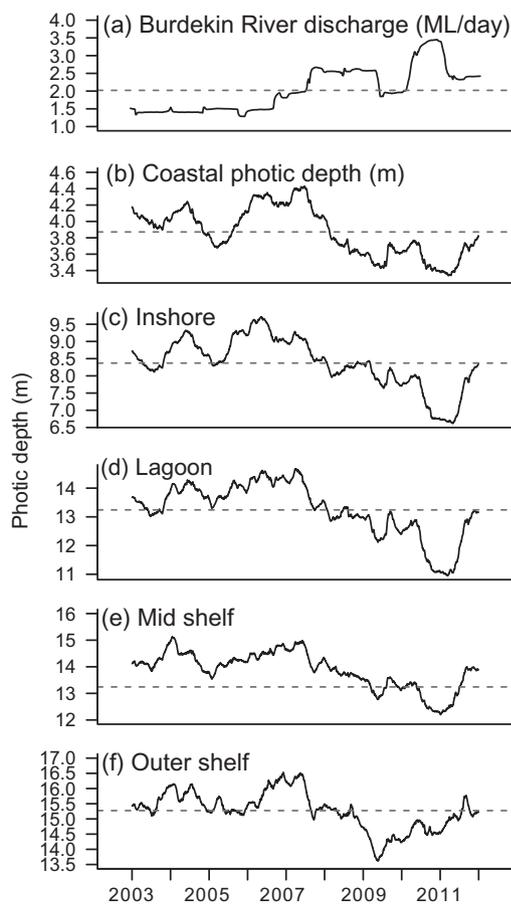
Fig. 6. Ten-year long-term trend in daily Burdekin River discharge (a) and daily mean photic depth from 2002 through 2012 for the five bands across the continental shelf within the central GBR (b–f). The horizontal dashed lines indicate the mean value of each data set.

there on, photic depth started to increase again near-monotonously over a period of about four to five months, and returned to its maximum levels in the mid to late dry season (Table 2, Fig. 7). Regional daily mean photic depth was therefore reduced, from its dry season maximum, for about six to eight months after the Burdekin started flowing, included an approximately four months long period after the river discharges had subsided.

4. Discussion

This study demonstrates that river discharges strongly determine intra- and inter-annual variation in water clarity on a shallow tropical continental shelf such as the central GBR. Previous studies have demonstrated causal links between land use and river loads (e.g., Kuhnert et al., 2012; Waterhouse et al., 2012; Wilkinson et al., 2013), while numerous other studies have established strong links between GBR water clarity and the health of its ecosystems (e.g., Fabricius and De'ath, 2004; Cooper et al., 2007; Brodie et al., 2011; Fabricius et al., 2012; Brodie and Waterhouse, 2012). This study bridges these two bodies of research, by demonstrating strong associations between river loads and marine water clarity at regional scales. It shows that river runoff affects not only inshore water clarity, but that its effects extend all the way across the lagoon and into the midshelf bands (up to ∼80 km from the coast), where extensive deep-water seagrass meadows and many of the ∼2000 coral reefs of the GBR are located. After controlling for the daily effects of the obvious known environmental drivers (waves, tides and bathymetry; Larcombe and Woolfe, 1999; Anthony et al., 2004; Fabricius et al., 2013) and testing for time lags, we were able to detect a strong underlying seasonal cycle in photic depth. Furthermore, the strong long-term relationship between photic depth and discharge volumes became apparent after removing the seasonal cycle. Averaged across the whole shelf, annual mean photic depth was ∼20% reduced (and below water quality guideline values for 156 rather than 9 days) in the six wet compared to four dry years. A 20% reduction represents a significant loss of light as a resource for photosynthetic organisms such as corals and seagrasses (Anthony and Hoegh-Guldberg, 2003; Collier et al., 2012; Cooper and Ulstrup, 2009).

Within the coastal band (from the shore to ∼13 km), the relatively weak relationship between runoff and water clarity suggests that winnowing of new sediments takes longer than one seasonal cycle. Indeed, an up to 10-fold reduction in long-term mean water clarity on coastal and inshore reefs near compared to away from
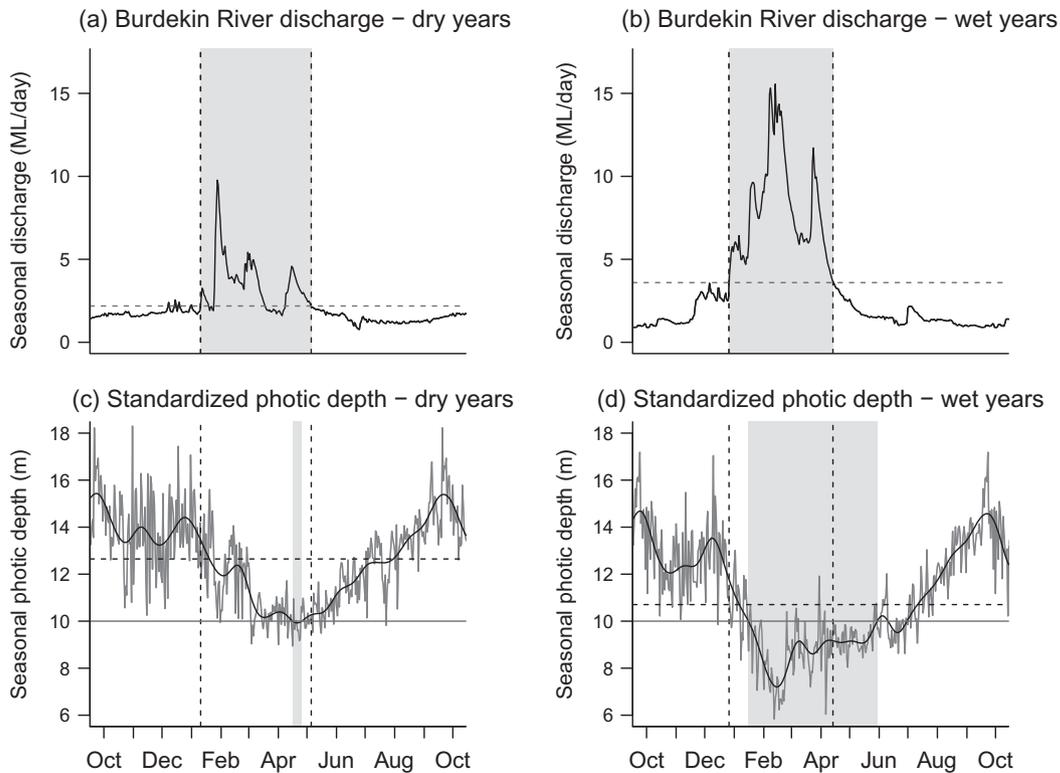
Fig. 7. Ten-year seasonal cycle in daily Burdekin River discharge (a and b) and daily, standardized mean photic depth (c and d) for the Burdekin region for the dry years (2003–2006) and the wet years (2007–2012). 'Standardized photic depth' represents back-transformed values after having removed the effects of wave height, wave frequency, tidal range and bathymetry. The black solid lines represent a β-spline smoother and the grey traces are the (scaled) first order derivatives of the smoothing function. The horizontal dashed lines indicate an arbitrary split (mean value) between high and low values for the dry and wet years, respectively. The shaded underlays represent periods with above-mean levels of discharge, and periods below the 10-m Secchi depth GBRMPA guideline value (grey horizontal line), respectively. Dashed vertical bars extend the region of high river discharge values onto the water clarity trace. Following seasonal decomposition of the GAMM residuals, seasonal trends were re-centered to the mean of water clarity predicted from the GAMM.

rivers suggests that fine river-derived sediments remain available for resuspension for years after floods (Fabricius et al., 2013). Thick deposits of predominantly terrigenous sediments have accumulated particular downstream of rivers at geological time scales (Belperio, 1983; Lambrechts et al., 2010), leading to assertions that GBR water clarity is not limited by modern sediment supply (e.g., Larcombe and Woolfe, 1999). However, our study showed that the new materials significantly contributed to reducing water clarity even in the coastal band (in wet years more than in dry years), i.e., that the geological deposits together with newly imported materials additively determined its water clarity.

For coastal and inshore reefs of the GBR, turbidity logger data have previously shown that water clarity was on average 43% higher at the end compared with the beginning of the dry season (Fabricius et al., 2013). In other words, as the floods subsided and the dry season progressed it required an increasing amount of wave and tidal energy to resuspend bottom sediments in the more turbid areas of the GBR. Three mechanisms may underpin this decay: (1) gradual transport of fine particulate materials and flocs towards deeper waters where resuspension requires higher wave and tidal energies, (2) sediment compaction and break-down of organic flocs and (3) declining plankton biomass after the depletion of nutrients and trace elements in the cooler winter months (Brodie et al., 2007; Lambrechts et al., 2010). The turbid shelf waters of the GBR (classified as 'case 2') are assumed to be typically dominated by detritus and abiotic suspended sediment particles rather than phytoplankton (Kirk, 1991), but plankton blooms develop in response to the runoff of new nutrients, iron and other trace elements (McKinnon and Thorrold, 1993; Smith and Schindler, 2009), and to nutrient release from sediment resuspension (Walker,

1981). However, the relative contributions of phytoplankton and flocculation to the observed changes in water clarity remain presently unknown.

For outer shelf water clarity, the causes for the weak but apparent relationship to river discharges remained unresolved. Plumes of the Burdekin River frequently extend to the midshelf, as shown by MODIS-Aqua data (Bainbridge et al., 2012; Devlin et al., 2012; Schroeder et al., 2012), and nepheloid transport and storms transport resuspended materials offshore throughout the year. To date, the short- and long-term rates of offshore transport of these materials through plumes, nepheloid flows and storms remain unknown. Phytoplankton concentrations decrease from the coast to the outer shelf, but also vary seasonally, with highest mean chlorophyll concentrations in the late wet season (March) and lowest in August (Brodie et al., 2007). High offshore water clarity in the central GBR during the late dry season has also been attributed to intrusions of oligotrophic offshore surface waters due to seasonal relaxation of the southeast trade winds and strengthening of the East Australian Current (Weeks et al., 2012). The relative contributions of phytoplankton and intrusions to determining water clarity are unknown, but both may contribute to explaining intra-annual differences in mid- and outer shelf water clarity. As the analyses had removed seasonal cycles, the residual patterns (e.g., differences between the wetter and dryer years) appear to indicate additional yet attenuated and lagged links to river processes.

The available data did not allow to differentiate between the relative effects of the different flood plume component (freshwater, TSS or nutrients). Although the analyses showed stronger associations of photic depth to freshwater discharge volumes and loads

of total phosphorus than to loads of nitrogen or total suspended solids, it has to be noted that such comparison was affected by a limited availability of river nutrient and sediment data: first, TP and TN load data were not available for the years 2003, 2004 and 2012, while TSS estimates were derived from different sources for different years, potentially affecting comparability (Table 1). Second, for TSS, the clay and fine silt fractions (in combination with nutrients) affect water clarity more than coarser grain sizes, and their relative contributions to TSS loads vary between floods (typically ~70–90%, depending on the origin from different subcatchments; Bainbridge et al., 2012; Lewis et al., 2013). Third, true TN loads are underestimated by an unknown factor as they do not include nitrate derived from extensive sugarcane areas below the gauging station. Also, TN contains typically an only small proportion (5–50%) in particulate compared to dissolved forms (Bainbridge et al., 2012; Kroon et al., 2012). In contrast, 60–80% of the TP load of the Burdekin River is in particulate rather than dissolved form (Bainbridge et al., 2012; Kroon et al., 2012). For this reason, TP appears the best proxy to estimate the fine fraction of TSS, and apparently the best predictor of the loss in photic depth.

The slopes of the relationship between photic depth and river discharges suggest that annual mean photic depth across the shelf was reduced by 1.7% for each 1000 tonnes of TP discharged into the GBR, or by 0.47% for each 1000 tonnes of TN. Indeed, our calculations suggest that predicted annual mean photic depth would increase by 4.8%, 5.9%, 5.3% and 3.5% in the coastal, inshore, lagoon and midshelf bands for a 50% reduction in TP loads in the Burdekin River. These gains would be unevenly distributed across the year, with gains exceeding the annual means from February to July, and smaller benefits in the remaining months (Table 2). Although a 50% reduction may appear substantial, it is a relatively modest target compared with the ~6-fold increases of TP that has occurred since pre-European times (Kroon et al., 2012). The model predicts similar gains for a 50% reduction in TN (4.1%, 5.5%, 4.7% and 2.9%). However, annual mean values of TP and TN are highly correlated ($R^2 = 0.94$), making it impossible to assess the relative merits of removal of either form of nutrients on water clarity. Strong interactive effects between dissolved nutrients and fine sediments, through the formation of organic rich flocs that remain easily resuspendible (Bainbridge et al., 2012), further highlight the difficulty to separating the relative effects of specific forms of nutrients and sediments.

In conclusion, our results show that river discharges significantly affect water clarity across the inshore, lagoonal and midshelf bands of the central GBR. The data suggest that a reduction in fine sediments and nutrient loads in the Burdekin River is likely to improve water clarity for six to eight months per year, potentially also providing cumulative benefits in consecutive years especially in the coastal band. The documented changes in water clarity are sufficiently large to affect coral reef and seagrass communities, hence reductions in river loads would likely lead to substantial ecosystem health benefits. Total suspended solid concentrations in the Burdekin River increase by 2.1% with each percentage loss in vegetation cover (Kuhnert et al., 2012), suggesting that more effective vegetation management especially in dry years will have a significant impact on water clarity in the central GBR. Specific sub-catchments that contribute most to the sediment and nutrient loads have been identified, and the relative roles of fertilizers, hillslope, gully and streambank erosion to end-of-river loads have been quantified (Waterhouse et al., 2012; Wilkinson et al., 2013). Land management efforts should therefore be prioritised to maximize the retention of nutrients, clays and fine silts in these sub-catchments, which would not only safe-guard the long-term productivity of farms, but also improve water clarity and ecosystem health in the central GBR, suggesting a win–win situation. Importantly, our data suggest that improvements in water clarity

should be detectable both by river and inshore water quality monitoring programs at intra- to inter-annual time scales. The time frames for GBR coral reefs to recover from past and present exposure to poor water quality will however most certainly be slower, due to the relatively slow processes governing shifts in communities in coral reefs.

Appendix A. Supplementary material

Supplementary data associated with this article can be found, in the online version, at http://dx.doi.org/10.1016/j.marpolbul.2014.05.012.

References

Anthony, K., Ridd, P.V., Orpin, A.R., Lough, J., 2004. Temporal variation of light availability in coastal benthic habitats: effects of clouds, turbidity, and tides. Limnol. Oceanogr. 49, 2201–2211.

Anthony, K.R., Hoegh-Guldberg, O., 2003. Kinetics of photoacclimation in corals. Oecologia 134, 23–31.

Bainbridge, Z., Wolanski, E., Lewis, S., Brodie, J., 2012. Fine sediment and nutrient dynamics related to particle size and floc formation in a Burdekin River flood plume, Australia. Mar. Pollut. Bull. 65, 236–248.

Beaman, R.J., 2012. Great barrier reef and coral sea bathymetry. James Cook University. <http://deepreef.org>.

Belperio, A.P., 1983. Terrigenous sedimentation in the central Great Barrier Reef lagoon: a model from the Burdekin region. BMR J. Aust. Geol. Geophys. 8, 179–190.

Belperio, A.P., Searle, D.E., 1988. Terrigenous and carbonate sedimentation in the Great Barrier Reef province. In: J, D.L., H, R.H. (Eds.), Carbonate to Clastic Facies Changes. Developments in Sedimentology. Elsevier Science Publishers, Amsterdam, pp. 143–174.

Birkeland, C., 1988. Geographic comparisons of coral-reef community processes, In: Choat, J.H., Barnes, D., Borowitzka, M., Coll, J.C., Davies, P.J., Flood, P., Hatcher, B.G., Hopley, D., Hutchings, P.A., Kinsey, D.W., Orme, G.R., Pichon, M., Sale, P.F., Sammarco, P.W., Wallace, C.C., Wilkinson, C., Wolanski, E., Bellwood, O. (Eds.), Proceedings of the 6th International Coral Reef Symposium, Townsville, pp. 211–220.

Brodie, J., De'ath, G., Devlin, M., Furnas, M., Wright, M., 2007. Spatial and temporal patterns of near-surface chlorophyll a in the Great Barrier Reef lagoon. Mar. Freshwater Res. 58, 342–353.

Brodie, J., Schroeder, T., Rohde, K., Faithful, J., Masters, B., Dekker, A., Brando, V., Maughan, M., 2010. Dispersal of suspended sediments and nutrients in the Great Barrier Reef lagoon during river-discharge events: conclusions from satellite remote sensing and concurrent flood-plume sampling. Mar. Freshwater Res. 61, 651–664.

Brodie, J., Waterhouse, J., 2012. A critical review of environmental management of the 'not so Great' Barrier Reef. Coast. Estuar. Shelf Sci. 104, 1–22.

Brodie, J., Wolanski, E., Lewis, S.E., Bainbridge, Z., 2012. An assessment of residence times of land-sourced contaminants in the Great Barrier Reef lagoon and the implications for management and reef recovery. Mar. Pollut. Bull. 65, 267–279.

Brodie, J., Devlin, M., Haynes, D., Waterhouse, J., 2011. Assessment of the eutrophication status of the Great Barrier Reef lagoon (Australia). Biogeochemistry 106, 281–302.

Collier, C., Waycott, M., Ospina, A.G., 2012. Responses of four Indo-West Pacific seagrass species to shading. Mar. Pollut. Bull. 65 (65), 342–354.

Cooper, T.F., Ulstrup, K.E., 2009. Mesoscale variation in the photophysiology of the reef building coral *Pocillopora damicornis* along an environmental gradient. Estuar. Coast. Shelf Sci. 83, 186–196.

Cooper, T.F., Uthicke, S., Humphrey, C., Fabricius, K.E., 2007. Gradients in water column nutrients, sediment parameters, irradiance and coral reef development in the Whitsunday region, central Great Barrier Reef. Estuar. Coast. Shelf Sci. 74, 458–470.

De'ath, G., Fabricius, K.E., 2010. Water quality as a regional driver of coral biodiversity and macroalgae on the Great Barrier Reef. Ecol. Appl. 20, 840–850.

Devlin, M.J., McKinna, L.C., Alvarez-Romero, J.G., Petus, C., Abott, B., Harkness, P., Brodie, J., 2012. Exposure to riverine plumes in the Great Barrier Reef. Risk assessment by mapping plume extent and composition using remote sensing. Mar. Pollut. Bull. 65, 224–235.

Doron, M., Babin, M., Hembise, O., Mangin, A.P.G., 2011. Ocean transparency from space: validation of algorithms estimating secchi depth using MERIS, MODIS and SeaWiFS data. Remote Sens. Environ. 115, 2986–3001.

Duarte, C.M., 1991. Seagrass depth limits. Aquat. Bot. 40, 363–377.

Eilers, P., Rijnmond, D., Marx, B., 1996. Flexible smoothing with B-splines and penalties. Stat. Sci. 11, 89–121.

Fabricius, K., De'ath, G., Humphrey, C., Zagorskis, I., Schaffelke, B., 2013. Intra-annual variation in turbidity in response to terrestrial runoff at near-shore coral reefs of the Great Barrier Reef. Estuar. Coast. Shelf Sci. 116, 57–65.

Fabricius, K.E., Cooper, T.F., Humphrey, C., Uthicke, S., De'ath, G., Davidson, J., LeGrand, H., Thompson, A., Schaffelke, B., 2012. A bioindicator system for water quality on inshore coral reefs of the Great Barrier Reef. Mar. Pollut. Bull. 65, 320–332.

Fabricius, K.E., De'ath, G., 2004. Identifying ecological change and its causes: a case study on coral reefs. Ecol. Appl. 14, 1448–1465.

Flater, D., 2007. XTide v2:harmonic tide clock and tide predictor. http://www.flaterco.com/xtide/.

Gagan, M.K., Chivas, A.R., Herczeg, A.L., 1990. Shelf wide erosion, deposition and suspended sediment transport during cyclone Winifred, central Great Barrier Reef, Australia. J. Sediment. Petrol. 60, 456–470.

Great_Barrier_Reef_Marine_Park_Authority, 2009. Water Quality Guidelines for the Great Barrier Reef Marine Park. Great Barrier Reef Marine Park Authority, Townsville.

IOCCG, 2006. Remote Sensing of Inherent Optical Properties: Fundamentals, Tests of Algorithms, and Applications. In: Lee, Z. (Ed.). Reports of the International Ocean-Colour Coordinating Group, Dartmouth, Canada, p. 126.

Kendall, M., Stuart, A., 1983. The Advanced Theory of Statistics. Charles Griffin and Company, London.

Kirk, J., 1991. Volume scattering function, average cosines, and the underwater light field. Limnol. Oceanogr. 36, 455–467.

Kroon, F.J., Kuhnert, P.M., Henderson, B.L., Wilikinson, S.N., Kinsey-Henderson, A., Brodie, J.E., Turner, R.D.R., 2012. River loads of suspended solids, nitrogen, phosphorus and herbicides delivered to the Great Barrier Reef lagoon. Mar. Pollut. Bull. 65, 167–181.

Kuhnert, P.M., Henderson, B., Lewis, S.E., Bainbridge, Z.T., Wilkinson, S.N., Brodie, J.E., 2012. Quantifying total suspended sediment export from the Burdekin River catchment using the loads regression estimator tool. Water Resour. Res. 48, W04533.

Lambrechts, J., Humphrey, C., McKinna, L., Gourge, O., Fabricius, K.E., Mehta, A.J., Lewis, S., Wolanski, E., 2010. Importance of wave-induced bed liquefaction in the fine sediment budget of Cleveland bay, Great Barrier Reef. Estuar. Coast. Shelf Sci. 89, 154–162.

Larcombe, P., Ridd, P.V., Prytz, A., Wilson, B., 1995. Factors controlling suspended sediment on inner-shelf coral reefs, Townsville, Australia. Coral Reefs 14, 163–171.

Larcombe, P., Woolfe, K., 1999. Increased sediment supply to the Great Barrier Reef will not increase sediment accumulation at most coral reefs. Coral Reefs 18, 163–169.

Lee, Z., Carder, K.L., Arnone, R.A., 2002. Deriving inherent optical properties from water color: a multiband quasi-analytical algorithm for optically deep waters. Appl. Opt. 41, 5755–5772.

Lee, Z., Weidemann, A., Kindlemann, J., Arnone, R., Carder, K.L., Davis, C., 2007. Euphotic zone depth: its derivation and implication to ocean-color remote sensing. Geophys. Res. 112, C3.

LeGrand, H.M., Fabricius, K.E., 2011. Relationship of internal macrobioeroder densities in living massive *Porites* to turbidity and chlorophyll on the Australian Great Barrier Reef. Coral Reefs 2011, 97–107.

Lewis, S., Bainbridge, Z., Kuhnert, P., Sherman, B., Henderson, B., Dougall, C., Cooper, M., Brodie, J., 2013. Calculating sediment trapping efficiencies for reservoirs in tropical settings: a case study from the Burdekin Falls Dam, NE Australia. Water Resour. Res. 49, 1017–1029.

McKinnon, A.D., Thorrold, S.R., 1993. Zooplankton community structure and copepod egg production in coastal waters of the central Great Barrier Reef lagoon. J. Plankton Res. 15, 1387–1411.

Orpin, A.R., Brunskill, G.J., Zagorskis, I., Woolfe, K.J., 2004. Patterns of mixed siliciclastic–carbonate sedimentation adjacent to a large dry-tropics river on the central Great Barrier Reef shelf, Australia. Aust. J. Earth Sci. 51, 665–683.

Pinheiro, J., Bates, D., 2000. Mixed Effects Models in S and S-PLUS. Springer-Verlag, New York.

Piniak, G.A., Storlazzi, C.D., 2008. Diurnal variability in turbidity and coral fluorescence on a fringing reef flat: Southern Molokai, Hawaii. Estuar. Coast. Shelf Sci. 77, 56–64.

Queensland, S.O., 2013. Reef Water Quality Protection Plan – Second Report Card. Queensland Government.

R_Development_Core_Team, 2013. R: A Language and Environment for Statistical Computing. R Foundation for Statistical Computing, Vienna, Austria.

Saulquin, B., Hamdi, A., Gohin, F., Populus, J., Mangin, A., D'Andon, O.F., 2013. Estimation of the diffuse attenuation coefficient K-dPAR using MERIS and application to seabed habitat mapping. Remote Sens. Environ. 128, 224–233.

Schroeder, T., Devlin, M., Brando, V.E., Dekker, A.G., Brodie, J., Clementson, L.A., McKinna, L., 2012. Inter-annual variability of wet season freshwater plume extent in the Great Barrier Reef lagoon based on satellite coastal ocean colour observations. Mar. Pollut. Bull. 65, 210–223.

Smith, V.E., Schindler, D.W., 2009. Eutrophication science: where do we go from here? Trends Ecol. Evol. 24, 201–207.

Storlazzi, C.D., Field, M.E., Bothner, M.H., Presto, M.K., Draut, A.E., 2009. Sedimentation processes in a coral reef embayment: Hanalei Bay, Kauai. Mar. Geol. 264, 140–151.

Storlazzi, C.D., Jaffe, B.E., 2008. The relative contribution of processes driving variability in flow, shear, and turbidity over a fringing coral reef: West Maui, Hawaii. Estuar. Coast. Shelf Sci. 77, 549–564.

The_State_of_Queensland_and_Commonwealth_of_Australia, 2009. Reef Water Quality Protection Plan for catchments adjacent to the Great Barrier Reef World Heritage Area. Queensland Department of Premier and Cabinet, Brisbane.

Walker, T.A., 1981. Dependence of phytoplankton chlorophyll on bottom resuspension in Cleveland Bay, northern Queensland. Aust. J. Mar. Freshwater Res. 32, 981–986.

Waterhouse, J., Brodie, J., Lewis, S., Mitchell, A., 2012. Quantifying the sources of pollutants in the Great Barrier Reef catchments and the relative risk to reef ecosystems. Mar. Pollut. Bull. 65, 394–406.

Weeks, S., Werdell, P.J., Schaffelke, B., Canto, M., Lee, Z., Wilding, J.G., Feldman, G.C., 2012. Satellite-derived photic depth on the Great Barrier Reef: spatio-temporal patterns of water clarity. Remote Sens. 4, 3781–3795.

Wilkinson, S.N., Hancock, G.J., Bartley, B., Hawdon, A.A., Keen, R., 2013. Using sediment tracing to assess processes and spatial patterns of erosion in grazed rangelands, Burdekin River basin, Australia. Agric. Ecosyst. Environ. 180, 90–102.

Wolanski, E., Fabricius, K., Cooper, T., Humphrey, C., 2008. Wet season fine sediment dynamics on the inner shelf of the Great Barrier Reef. Estuar. Coast. Shelf Sci. 77, 755–762.

Wolanski, E., Fabricius, K., Spagnol, S., Brinkman, R., 2005. Fine sediment budget on an inner-shelf coral-fringed island, Great Barrier Reef of Australia. Estuar. Coast. Shelf Sci. 65, 153–158.

Wolanski, E., Marshall, K., Spagnol, S., 2003. Nepheloid layer dynamics in coastal waters of the Great Barrier Reef, Australia. J. Coast. Res. 19, 748–752.

Wood, S.N., 2006. In: Generalized Additive Models: An Introduction with R. Chapman and Hall/CRC Press.

Wood, S.N., 2011. Fast stable restricted maximum likelihood and marginal likelihood estimation of semiparametric generalized linear models. J. R. Stat. Soc. Ser. B 73, 3–36.

Zhao, J., Barnes, B., Melo, N., English, D., Lapointe, B., Muller-Karger, F., Schaeffer, B.C.H, 2013. Assessment of satellite-derived diffuse attenuation coefficients and euphotic depths in south Florida coastal waters. Remote Sens. Environ. 131, 38–50.